

# Elastoviscoplastic rheology and aging in a simplified soft glassy constitutive model

Suzanne M. Fielding

Citation: *Journal of Rheology* **64**, 723 (2020); doi: 10.1122/1.5140465

View online: <https://doi.org/10.1122/1.5140465>

View Table of Contents: <https://sor.scitation.org/toc/jor/64/3>

Published by the [The Society of Rheology](#)

---

## ARTICLES YOU MAY BE INTERESTED IN

[reptate rheology software: Toolkit for the analysis of theories and experiments](#)

*Journal of Rheology* **64**, 709 (2020); <https://doi.org/10.1122/8.0000002>

[Influence of hydrostatic pressure on rheological properties of polymer melts—A review](#)

*Journal of Rheology* **64**, 751 (2020); <https://doi.org/10.1122/1.5142059>

[Evaluating the exit pressure method for measurements of normal stress difference at high shear rates](#)

*Journal of Rheology* **64**, 739 (2020); <https://doi.org/10.1122/1.5145255>

[Evaluating predictability of various constitutive equations for MAOS behavior of entangled polymer solutions](#)

*Journal of Rheology* **64**, 673 (2020); <https://doi.org/10.1122/1.5139685>

[Stress decomposition in LAOS of dense colloidal suspensions](#)

*Journal of Rheology* **64**, 343 (2020); <https://doi.org/10.1122/1.5144520>

[A review of thixotropy and its rheological modeling](#)

*Journal of Rheology* **63**, 477 (2019); <https://doi.org/10.1122/1.5055031>

---



**DISCOVER** the **RHEOMETER** with the...  
**Sensitivity • Ease-of-use • Versatility**  
to address the most **demanding** applications

The **NEW Discovery Hybrid Rheometer**





# Elastoviscoplastic rheology and aging in a simplified soft glassy constitutive model

Suzanne M. Fielding<sup>a)</sup>

Department of Physics, Durham University, Science Laboratories, South Road, Durham DH1 3LE, United Kingdom

(Received 27 November 2019; final revision received 20 January 2020; published 9 April 2020)

## Abstract

Yield stress fluids display a rich rheological phenomenology. Beyond the defining existence of a yield stress in the steady state flow curve, this includes, in many materials, rather flat viscoelastic spectra over many decades of frequency in small amplitude oscillatory shear; slow stress relaxation following the sudden imposition of a small shear strain; stress overshoot in shear startup; logarithmic or sublinear power-law creep following the imposition of a shear stress below the yield stress; creep followed by yielding after the imposition of a shear stress above the yield stress; richly featured Lissajous–Bowditch curves in large-amplitude oscillatory shear; a Bauschinger effect, in which a material's effective yield strain is lowered under straining in one direction, following a preceding strain in the opposite direction; hysteresis in up-down shear rate sweeps; and (in some materials) thixotropy and/or rheological aging. A key challenge is to develop a constitutive model that contains enough underlying mesoscopic physics to have meaningful predictive power for the full gamut of rheological behavior just described, with only a small number of model parameters, yet is simple enough for use in computational fluid dynamics to predict flows in complicated geometries, or complicated flows that arise due to spontaneous symmetry breaking instabilities even in simple geometries. Here, we introduce such a model, motivated by the widely used soft glassy rheology model, and show that it captures all the above rheological features. © 2020 The Society of Rheology. <https://doi.org/10.1122/1.5140465>

## I. INTRODUCTION

Many soft materials behave as so-called “yield stress fluids” [1–8]. Examples include dense colloids, emulsions, foams, star polymers, microgels, and lamellar onion phases, as well as low density attractive colloidal gels and clays. At imposed stresses below a critical yield stress,  $\sigma < \sigma_y$ , they show solidlike rheological behavior. In contrast, at larger stresses,  $\sigma > \sigma_y$ , they yield and flow like liquids. Their steady state flow curve of shear stress  $\sigma$  as a function of shear rate  $\dot{\gamma}$ , typically measured in a slow shear rate sweep, is then often fit to a Herschel–Bulkley form [9],  $\sigma(\dot{\gamma}) = \sigma_y + K\dot{\gamma}^n$ , with  $0 < n < 1$ , or Bingham behavior [10] with  $n = 1$ .

In terms of the physical origin of this behavior, yield stress fluids can (broadly and loosely) be subdivided into two main categories. In the first category, a material's constituent mesoscopic substructures, such as colloidal particles, attract to form weakly flocculated aggregates [11]. Even though the volume fraction of the constituent particles can be quite low for the system overall, their aggregates can result in a gel-like response at low loads but are then pulled apart and refluidized in shear.

In the second category, a material's constituent substructures are too densely packed to properly rearrange at low loads but do rearrange in shear. Examples include colloids, emulsions, foams, microgels, etc., which, respectively, comprise densely packed colloidal particles, emulsion droplets, foam bubbles, or microgel beads. Materials in this second category can further be divided into (at least) two idealized limiting subcategories [12,13]: thermal hard-sphere colloids,

in which the yield stress has a typical magnitude  $k_B T/R^3$ , where  $R$  is the particle radius, and athermal soft suspensions, in which the yield stress has a typical magnitude set by the modulus of the constituent particles. Materials in the second subcategory have been termed “soft glassy materials” [14–16]. The constitutive model that we shall present in what follows is aimed, in particular, at dense athermal soft particle suspensions and motivated by the original, widely used “soft glassy rheology” (SGR) model [14–16]. It is worth noting, however, that the model actually also captures many of the observed rheological features of dense hard sphere colloids and of low density attractive gels.

Beyond the defining presence of a yield stress in the steady state flow curve, yield stress fluids also display a host of interesting *dynamic* rheological behaviors. In linear response, the viscoelastic spectra characterizing their stress response to a small amplitude oscillatory shear strain typically show a rather flat, power-law dependence over many decades of the oscillation frequency,  $\omega$  [17–23]. The storage modulus,  $G'(\omega)$ , typically exceeds the loss modulus,  $G''(\omega)$ , by about an order of magnitude, consistent with a nearly elastic response overall for these small deformations. The presence of nontrivial dissipation (a nonzero  $G''$ ) even at the lowest frequencies accessible experimentally, however, also reveals a broad underlying spectrum of sluggish stress relaxation modes. The stress decay following the sudden imposition of a small shear strain occurs over a similarly wide range of sluggish relaxation time scales [24].

The behavior of yield stress fluids in time-dependent nonlinear flows is similarly rich, in both strain-imposed and stress-imposed protocols. In shear startup from rest, for example, they typically display an initially elastic solidlike regime in which the stress increases linearly with strain up to

<sup>a)</sup>Electronic mail: [suzanne.fielding@durham.ac.uk](mailto:suzanne.fielding@durham.ac.uk)

a maximum “overshoot” value. Following this stress overshoot, the material yields and the stress declines to its value in the ultimate fluidized flowing state, prescribed by the steady state flow curve. Such behavior has been observed in foams [19], emulsions [25,26], Carbopol [27,28], Laponite [29,30], a fused silica suspension [31], attractive gels [32,33], and waxy crude oil [34].

Following the imposition of a step shear stress below the yield stress, a sustained solidlike slow creep response is typically seen, in which the strain increases logarithmically or as a sublinear power of time, with the strain rate accordingly decreasing as a power law. In this way, the material creeps forward at an ever slowing rate but never attains a steady flow of nonzero rate. Following the imposition of a shear stress just above the yield stress, in contrast, an early time creep regime is followed at later times by a dynamical yielding process in which the shear rate increases up to its final value prescribed by the steady state flow curve. Such behavior has been observed in Carbopol gel [35,36], carbon black [37–39], polycrystalline hexagonal columnar phases [40], and colloidal glasses [41,42].

Back-and-forth strain, strain rate or stress ramps, or oscillations have also been widely studied. In large-amplitude oscillatory shear (LAOS) experiments on yield stress fluids [43–57], parametric Lissajous–Bowditch (LB) plots of stress versus strain typically show a rather complicated progression in shape with increasing amplitude of the applied shear. For example, characteristic diamond-shaped LB curves are often seen for intermediate amplitudes. LB curves have recently been modeled within the SGR model in [58–60]. Yield stress materials often also display a Bauschinger effect [61,62], in which the apparent yield strain is reduced for straining in one direction, following a preceding plastic strain in the opposite direction. The stress response of yield stress fluids to shear rate sweeps often displays a pronounced hysteresis between the downward and upward sweeps, with the size of the hysteresis loop increasing with increasing sweep rate [63,64].

Indeed, the rheological response of many yield stress fluids also shows a pronounced dependence on the “waiting time” since a sample was prepared, before a flow is applied. This phenomenon is often termed rheological aging and/or thixotropy. For a precise definition of rheological aging, see [15]. The definition of thixotropy and its distinction from viscoelasticity and from aging is a topic of ongoing discussion [11]. Typically, a sample that has waited longer in an undisturbed state before a flow is applied will show a higher viscosity and/or a more solidlike response. The latter can be evidenced, for example, by a slower relaxation of stress following the rapid imposition of a small shear strain or a larger stress overshoot in shear startup in older samples. Typically, a material is then rejuvenated to a state of lower viscosity and/or lower solidity by an imposed flow.

During the dynamical process whereby a material yields from an initially solidlike to finally fluidlike state, a state of initially homogeneous shear will often become unstable to the formation of heterogeneous shear bands. This has been observed experimentally in yield stress fluids during shear startup [27–31,34], step stress [35–38,41], flow curve sweeps [64], and LAOS [53–55,57]. It has also been studied

theoretically and computationally in these same protocols of shear startup [65–76], step stress [72,77,78], flow curve sweeps [63], and LAOS [59,60]. In many materials, the shear bands that form during yielding then gradually heal away to leave a homogeneous steady flowing state. Some yield stress fluids instead support shear bands in the ultimate steady flowing state [79,80]. We do not consider such materials here: the model that we discuss has a monotonically increasing constitutive relation between stress and strain rate, precluding steady state shear banding.

From a theoretical viewpoint, a key challenge is to understand how the macroscopic flow properties just described emerge out of the underlying collective dynamics of a material’s constituent mesoscopic substructures, for any given category of yield stress fluids, and to build this understanding into a rheological constitutive model. Ideally, such a model should contain enough of the key mesoscopic physics to have meaningful predictive power for the full gamut of observed rheological phenomena, with just a small number of model parameters. At the same time, it should also be simple enough for use in computational fluid dynamics (CFD) to address flows in complicated geometries, or complicated flows that arise via spontaneous symmetry breaking instabilities even in simple geometries. It should, therefore, preferably be of the time-differential form, which is much easier to implement numerically in a CFD solver than a model of time-integral form. The primary contribution of this work is to introduce a constitutive model that for the first time, to the author’s knowledge, meets all these desirable criteria.

We start in Sec. II by briefly reviewing some of the most widely used models of yield stress rheology in the existing literature. In Sec. III, we discuss one such model in more detail: the SGR model. This does capture all the rheological phenomena described above but is in its present form far too complicated for use in CFD. Indeed, even computations of homogeneous simple shear flows can be very cumbersome within the SGR model in its existing form. Accordingly, in Sec. IV, we introduce a simplified SGR model, and in Sec. V, we demonstrate it to indeed capture all the rheological features discussed above. The potential contributions of this new model are twofold. First, it will allow significantly more straightforward computation of homogeneous shear flows for anyone wishing to fit the SGR model’s predictions to rheometric data. Second, it renders SGR feasible for use in CFD, once suitably tensorialized. Therefore, we suggest a possible generalization to tensorial stresses in Sec. VI, before finally setting out our conclusions in Sec. VII.

## II. OVERVIEW OF EXISTING CONSTITUTIVE MODELS

Existing elastoviscoplastic constitutive models range from those built from bottom up on the basis of microscopic or mesoscopic physics to those posed from top-down on the basis of macroscopic phenomenology. We now summarize some of the most widely used models in the existing literature and the extent to which they meet the desirable criteria set out in the penultimate paragraph of Sec. I.

### A. Microscopically derived models

For dense colloidal suspensions, a rheological constitutive theory has been built on the mode coupling theory (MCT) of the colloidal glass transition [81,82]. It starts by writing an equation of motion for the microscopic probability distribution in configuration space of the position vectors of a dense ensemble of Brownian particles (ignoring hydrodynamic interactions). This microscopic equation is then projected via a series of approximations onto a time-integral rheological constitutive equation for macroscopic stresses. This takes as its basic input the material's static and dynamic structure factors for the underlying microscopic density correlation functions.

MCT successfully captures many of the observed rheological features of dense colloidal suspensions, including the existence of a yield stress in the flow curve. Its formalism is heavy to implement in computational practice, however, even in simple homogeneous shear flows. Nonetheless, very recent work has incorporated a simplified schematic—although still time-integral—MCT constitutive equation into a lattice Boltzmann solver for CFD in the channel shear flow, assuming translational invariance in the flow direction [83].

### B. Mesoscopic elastoplastic models

Mesoscopic elastoplastic models conceptually divide a macroscopic sample of material into many local mesoscopic regions, each of which is ascribed continuum variables of local strain and stress relative to a locally undisturbed equilibrium. Each such region is represented as an elastoplastic element that loads elastically in the flow up to a local threshold, after which it yields plastically, then assumes a new elastic state relative to a new locally undeformed equilibrium.

In lattice-based elastoplastic models [84], the elements just described reside on a lattice, and the stress relaxation involved in any local plastic yielding event results in an explicit redistribution of stress to surrounding elements via an Eshelby propagator, ensuring that force balance is properly maintained [85]. Such models capture many observed features of elastoplastic rheology (even though they often fail properly to account for the advection of an element's position in the flow). In containing detailed spatial information about stress propagation, however, they are too computationally intensive in their present form for use in CFD to predict flows in anything other than small and simply shaped geometries.

Mean-field elastoplastic models instead discard any explicit spatial information about the location of elements and the stress propagation that follows local yielding events. Instead, they model stress propagation in a mean-field way. For example, the Hebraud–Lequeux model does so by invoking a diffusive term in the equation of motion for the probability distribution of local strains, with a diffusion constant set by the sample-average yielding rate [86]. Mean-field models with broader-tailed stress propagation statistics have also been studied [87]. Most such models, and their lattice-based counterparts described above, assume a flat distribution of local yield energy thresholds.

The SGR model [14–16] instead assumes a distribution of local yield energy thresholds with an exponential tail. It

furthermore models stress propagation by means of an effective temperature that can activate any element out of its local energy minimum and thereby trigger a local yielding event. This activation is taken to model, in a mean-field way, stress propagation from other local yielding events elsewhere in the sample. Starting from the initial purely mean-field model, SGR was later extended to address flows that develop spatial structuring in one spatial dimension, either via shear banding [88] or extensional necking [89], by allowing stress propagation in the relevant dimension.

Although the mean-field elastoplastic models just described are simpler than their lattice-based counterparts, they still, in general, involve the time evolution of a full distribution of local strain variables and remain as yet too complicated to implement in CFD.

An alternative mesoscopic approach, originally intended to model the deformation properties of metallic glasses, is based on the collective statistics of many “shear transformation zones” (STZs), which resemble the yielding local elements of the elastoplastic models just described [74,75].

### C. Phenomenological macroscopic models

Besides the microscopic and mesoscopic models just described, other constitutive models of yield stress rheology have been built from the top to down, on the basis of macroscopic phenomenology. The earliest such models posited a static relation between stress and strain rate [90–95]. When used in CFD, however, these necessitate a cumbersome separate calculation of the “yield surface” or regularization of sub-yield behavior [96]. They also miss most of the key physics, including all the dynamical rheological phenomena summarized in Sec. I.

More recent phenomenological models, therefore, instead posit an evolution equation for the stress, in order to account for the stress in a material at any time as a functional of the strain rate *history* it has experienced. This equation may depend on one or more auxiliary variables, for which evolution equations are also posited. Examples include fractional calculus [97,98], structural evolution, fluidity, and elastoviscoplastic models [34,56,99–104]. Although vastly superior to the static models, many involve 10–20+ fitting parameters, limiting their predictive power. Indeed, models benchmarked by fitting to straightforward strain-imposed protocols such as shear startup often then perform poorly in more complicated oscillatory/reversal protocols and/or in stress-imposed protocols. Furthermore, such models often incorporate phenomenological notions such as those of a “back-stress” or “kinematic hardening,” without always offering a clear understanding of such concepts in terms of the underlying microscopic or mesoscopic physics.

### D. Summary of existing models

Among the constitutive models just described, those based on underlying microscopic and mesoscopic physics tend to perform best at predicting the broad gamut of dynamical rheological phenomena described above, but they are often prohibitively complicated for use in CFD to predict macroscopic flows in complex geometries. In contrast, the macroscopic

phenomenological models are generally better suited to CFD but often contain many model parameters, and/or capture only a subset of the desired rheological phenomenology, and/or are limited in the underlying physics they contain.

Indeed, to the author's knowledge, no currently existing constitutive model of elastoviscoplastic yield stress rheology currently exists that satisfies all the desirable criteria set out above: of containing enough underlying micro/mesoscopic physics to predict the rich dynamical rheology of yield stress fluids with just a small number of model parameters, while also being simple enough—and preferably of time-differential form—for use in CFD to predict flows in complicated geometries.

### III. ORIGINAL SGR MODEL

The SGR model [14–16] considers an ensemble of elastoplastic elements, each representing a local mesoscopic region of soft glassy material (e.g., a few tens of emulsion droplets). Each element is assigned local continuum variables of shear strain  $l$  and shear stress  $kl$ , describing the mesoscopic region's state of elastic deformation relative to a locally undeformed equilibrium. In between local yielding events, the strain of each element affinely follows the macroscopic shear,  $\dot{l} = \dot{\gamma}$ , giving an elastic buildup of stress.

The stress is intermittently released by local plastic yielding events. In any such event, a mesoscopic region suddenly rearranges into a new configuration locally. This is modeled by its representative element hopping between traps in an energy landscape. An element in a trap of depth  $E$  and with local shear strain  $l$  is assigned a probability per unit time of hopping of  $\tau^{-1}(E, l)$ , with

$$\tau(E, l) = \tau_0 \exp\left[\left(E - \frac{1}{2}kl^2\right)/x\right]. \quad (3.1)$$

The stored elastic energy  $\frac{1}{2}kl^2$  at any instant, therefore, offsets the bare trap depth  $E$ , leading to a reduced local barrier to rearrangement,  $E - \frac{1}{2}kl^2$ . This confers rheological shear thinning on the sample as a whole. After hopping, an element selects a new trap depth at random from a prior distribution,

$$\rho(E) = \frac{1}{x_g} \exp(-E/x_g), \quad (3.2)$$

and resets its local strain  $l$  to zero, thereby relaxing the local stress.

With the dynamics just described, the probability  $P(E, l, t)$  for an element to be in a trap of depth  $E$  with local shear strain  $l$  evolves according to

$$\dot{P}(E, l, t) + \dot{\gamma} \frac{\partial P}{\partial l} = -\frac{1}{\tau(E, l)} P + Y(t) \rho(E) \delta(l). \quad (3.3)$$

The advected derivative on the left hand side captures the affine loading of each element by shear. The first (“death”) term on the right hand side describes hops out of traps. The

second (“birth”) term describes hops into the bottom of traps,  $l = 0$ , with the new trap depth chosen at random from the prior distribution,  $\rho(E)$ , and with an ensemble average hopping rate

$$Y(t) = \int dE \int dl \frac{1}{\tau(E, l)} P(E, l, t). \quad (3.4)$$

The macroscopic stress of the sample as a whole is defined as the average over the local elemental ones,

$$\sigma(t) = k \int dE \int dl l P(E, l, t). \quad (3.5)$$

Combined with the exponential prior,  $\rho(E)$ , the exponential activation factor  $\tau(E, l)$  confers a glass transition at a noise temperature  $x = x_g$ . In the absence of any applied flow, the model displays rheological aging in the glass phase [15],  $x < x_g$ : following sample preparation at time  $t = 0$  by means of a sudden quench from a high initial noise temperature to a value  $x < x_g$ , the system slowly evolves into ever deeper traps as a function of time  $t$ . This results in a growing stress relaxation time,  $\langle \tau \rangle \sim t$ , and, therefore, in ever more solidlike rheological response as the sample ages. An imposed shear of constant rate  $\dot{\gamma}$  will, however, arrest aging and rejuvenate the sample to a steady flowing state of effective age  $\langle \tau \rangle \sim 1/\dot{\gamma}$ . The steady state flow curve has a yield stress  $\sigma_y$  that grows linearly with  $x_g - x$  in the glass phase  $x < x_g$ .

For many soft glassy materials, the typical energy barrier for rearrangements greatly exceeds thermal energies. Accordingly, parameter  $x$  is not the true thermodynamic temperature but is taken as an effective noise temperature that models in a mean-field way coupling with other yielding events elsewhere in the sample.

As noted above, the SGR model captures a glass transition and aging by invoking the exponential form for the probability distribution of posthop yield-energies in Eq. (3.2). Recent particle based simulations explicitly measured the distribution of yield thresholds and local stresses for a sheared Lennard–Jones glass [105–107], see also [108]. It would clearly be interesting to undertake such a study for an athermal suspension of purely repulsive soft particles.

The full SGR model just described captures many features of the elastoplastic rheology of yield stress fluids. These include a yield stress in the steady state flow curve; broad and rather flat power-law viscoelastic spectra, aging in the power-law stress decay following a small amplitude step shear strain, an overshoot in the shear stress following the switch-on of a shear of constant rate  $\dot{\gamma}$ , slow creep during which the shear rate slowly decreases after the imposition of a shear stress below the yield stress, slow creep over several time decades followed by yielding and a sudden increase of the shear rate to a steady flowing state after the imposition of a shear stress just above the yield stress, and characteristic diamond or rhomboidal shaped Lissajous curves in a LAOS strain.

The ability of the SGR model to capture this rich rheological phenomenology within such a minimal and powerfully generic set of physical assumptions and with just one

free parameter—the noise temperature,  $x$ —is a remarkable achievement. Set against that achievement, this simplicity at the same time also inevitably limits the model’s ability to fit experimental data at a detailed *quantitative* level. As such, a worthwhile avenue for future study could be to bring in additional microscopic physics characterized by a small number of additional model parameters, potentially opening up the possibility of quantitatively fitting experimental data, while still keeping the number of model parameters and assumptions much smaller than in existing top-down phenomenological models. One such approach could be to build deformation and flow into a multilayer glassy trap model along the lines of that in [109].

We have described here the SGR model in its original form, which considers only scalarized shear stresses and which contains no spatial information about the location of any element. As such, it addresses only homogeneous simple shear flows. Extensions of the model have since been put forward to address tensorial stresses [110] and flows that become heterogeneous in one spatial dimension due to shear banding [88] or extensional necking [89].

#### IV. SIMPLIFIED SGR MODEL

##### A. Motivation for a simplified model

As noted above, the fact that the SGR model captures the rich phenomenology just described within a relatively simple and generic set of physical assumptions, and with a small number of model parameters, is a remarkable achievement. Indeed, once suitable units have been chosen, the model’s only free parameter is the noise temperature,  $x$ .

Set against this appeal is the considerably cumbersome task of computing these rheological behaviors in practice. Even for homogeneous simple shear flows, this requires the solution either of the full partial differential equation (PDE) given above,  $\partial_t P(E, l, t) = \dots$ , or the solution of two coupled nonlinear integral constitutive equations with power-law memory kernels (derived from the original PDE) [16], or the direct simulation of hopping SGR elements [60], typically with  $10^5$  elements required for reliable predictions. (This direct simulation is generally easier to implement computationally than a numerical solution of the differential or integral equations but is still costly in terms of computer time.)

To utilize the (tensorially extended) full SGR model in CFD to address heterogeneous flows in complicated geometries would require comparably involved computation at each lattice site: a task that is likely to prove prohibitively formidable in both practical implementation and computational cost. Indeed, to the author’s knowledge, such a task has not been attempted to date.

The present paper, therefore, aims to develop a simplified SGR model that captures the same rich phenomenology as the original model but with greatly reduced computational demand. The contributions of this will be twofold. First, the calculation of homogeneous flows will be made simpler for anyone wishing to compare rheometric experimental data with SGR. Second, the SGR model will be rendered simple enough for practical use in CFD for predicting elastoplastic flows in complicated geometries, or complicated flow patterns

that arise via spontaneous symmetry breaking instabilities even in simple geometries.

We shall undertake this simplification first in the context of a scalarized approach that considers only shear strains and stresses, before returning in Sec. VI to suggest a tensorial generalization, as needed for CFD.

##### B. Simplified model

We start by exactly rewriting the full SGR model equation, Eq. (3.3), as follows:

$$\dot{P}(E, l, t) + \dot{\gamma} \frac{\partial P}{\partial l} = -\frac{1}{\tilde{\tau}(E)} f(l) P + Y(t) \rho(E) \delta(l), \quad (4.1)$$

in which we have written the “bare” hopping time

$$\tilde{\tau}(E) = \tau_0 \exp\left(\frac{E}{x}\right) \quad (4.2)$$

and the “boost factor” to the hopping rate

$$f(l) = \exp\left(\frac{kl^2}{2x}\right). \quad (4.3)$$

We now exactly rewrite the full joint probability distribution  $P(E, l, t)$  of an element being in a trap of depth  $E$  with a local strain  $l$  as the probability  $G(E, t)$  of an element being in a trap of depth  $E$  multiplied by the conditional probability  $P_1(l|E, t)$  of an element having a local strain  $l$ , given that it is in a trap of depth  $E$

$$P(E, l, t) = G(E, t) P_1(l|E, t). \quad (4.4)$$

We have suggestively used the notation  $G(E, t)$  rather than  $P(E, t)$  in the first term on the right hand side because this quantity will assume the behavior of a moduluslike quantity (once redimensionalized by  $k$ ).

We can then exactly rewrite Eq. (4.1) as

$$\begin{aligned} \dot{G}(E, t) P_1 + G \dot{P}_1 + \dot{\gamma} G \frac{\partial P_1}{\partial l} \\ = -\frac{G}{\tilde{\tau}(E)} f(l) P_1 + Y(t) \rho(E) \delta(l). \end{aligned} \quad (4.5)$$

Averaging this equation over  $l$  at a fixed  $E$  then gives

$$\frac{d}{dt} G(E, t) = -\frac{G(E, t)}{\tilde{\tau}(E)} \overline{f(l)(E, t)} + Y(t) \rho(E). \quad (4.6)$$

Instead, premultiplying Eq. (4.5) by  $l$  before averaging over  $l$  at a fixed  $E$  gives the additional equation,

$$\frac{d}{dt} [G(E, t) \overline{l(E, t)}] = G(E, t) \dot{\gamma} - \frac{G(E, t)}{\tilde{\tau}(E)} \overline{l f(l)(E, t)}. \quad (4.7)$$

In these equations, we have used the notation

$$\overline{a(l)(E, t)} = \int dl P_1(l|E, t) a(l), \quad (4.8)$$

for any function  $a(l)$ .

Equations (4.6) and (4.7) together constitute an *exact* rewriting of the full SGR model. We now make an *approximation* by rewriting

$$\overline{a(l)} = a(\bar{l}). \quad (4.9)$$

This amounts to assuming that the distribution  $P_1(l|E, t)$  has the form of a delta function located at  $\bar{l}(E, t)$ , i.e., that traps of depth  $E$  have a single slaved local strain,  $\bar{l}(E, t)$ . For simplicity, we now further drop the overbar notation from  $l$ . Equations (4.6) and (4.7) can then be written as

$$\dot{G}(E, t) = -\frac{G(E, t)}{\tau(E, l(E, t))} + Y(t)\rho(E) \quad (4.10)$$

and

$$\dot{\sigma}(E, t) = kG(E, t)\dot{\gamma} - \frac{\sigma(E, t)}{\tau(E, l(E, t))}. \quad (4.11)$$

Here, we premultiplied Eq. (4.7) by  $k$  and have defined the stress in traps of depth  $E$ ,

$$\sigma(E, t) = kG(E, t)l(E, t). \quad (4.12)$$

The average hopping rate,

$$Y(t) = \int dE \frac{G(E, t)}{\tau(E, l(E, t))}, \quad (4.13)$$

with an  $E$ -dependent relaxation time scale

$$\tau(E, l(E, t)) = \tau_0 \exp\left[\left(E - \frac{1}{2}kl(E, t)^2\right)/x\right]. \quad (4.14)$$

Normalization of overall element numbers demands that

$$\int dE G(E, t) = 1. \quad (4.15)$$

As above, the prior distribution is

$$\rho(E) = \frac{1}{x_g} \exp(-E/x_g). \quad (4.16)$$

Throughout what follows, in both the original and simplified SGR models, we shall choose units of time in which  $\tau_0 = 1$  and of energy in which  $x_g = 1$ . We further rescale strains such that  $k = 1$ , making the typical yield strain of order unity.

### C. Discussion of the simplified model

The simplified SGR model just described has a rather appealing physical structure. Indeed, for any fixed value of energy depth  $E$ , Eq. (4.11) takes the form of a Maxwell model in which an elastic loading term with an effective modulus  $G(E, l)$  (in our units) competes with a plastic stress relaxation term. The relaxation time  $\tau(E, l(E))$  is, however, a strongly nonlinear function of the energy depth  $E$  and local strain  $l$ . The modulus,  $G(E, t)$ , which is prescribed by the

fraction of elements in traps of depth  $E$ , furthermore has its own dynamics given by Eq. (4.10).

In assuming a single value of the local strain  $l(E, t)$  for all elements in traps of a given energy depth  $E$ , we have reduced the PDE of the full SGR model,  $\partial_t P(E, l, t) = \dots$ , with two dynamical variables, to two equations,  $\partial_t G(E, t) = \dots$  and  $\partial_t \sigma(E, t) = \dots$ , each with just one dynamical variable. Neither equation now contains any derivatives with respect to  $E$ , further simplifying any numerics.

Nonetheless, one must still, in principle, evolve the two full functions  $G(E, t)$  and  $l(E, t)$  over time  $t$ . A second, pragmatic simplification, however, arises in recognizing that the continuous spectrum of energy values can be discretized on a grid of  $N$  values linearly distributed in a suitably chosen range  $0 \leq E \leq E_{\max}$ . This leaves  $2N$  differential equations, which, apart from the integral couplings of Eqs. (4.13) and (4.15), are “ordinary” in form.

Numerical results obtained within this simplified model then, in principle, need converging to the limit  $E_{\max} \rightarrow \infty$ ,  $N \rightarrow \infty$ . Once converged, the results show excellent agreement with all the qualitative predictions of the full SGR model, in every rheological protocol studied. Indeed, they show exact quantitative agreement in the regime of linear rheology. As we shall see below, however, the quantitative numbers can differ from full SGR typically by a worst-case factor of about 2 in the most nonlinear regime of protocols such as those in Figs. 3 and 4.

Given this quantitative discrepancy from full SGR, together with the fact that even full SGR, with its minimal—and, therefore, powerfully generic—set of physical assumptions, is anyway not expected to model any particular experimental sample in a fully quantitative way, we follow in our numerical computations below the pragmatic philosophy of taking the minimal value of  $N$  required to give convergence to the  $N \rightarrow \infty$  limit of the simplified model to within 1%. Typically, we find  $E_{\max} = 12.0$  and  $N = 32$  sufficient for most protocols. Indeed, even  $N = 16$  gives convergence to 5%, but we take  $N = 32$  minimally in what follows.

This brings the number of degrees of freedom required to predict homogeneous simple shear flows into the numerically trivial and represents a considerable simplification compared with the full SGR model, which required the solution of the full PDE  $\partial_t P(E, l, t) = \dots$ , or the solution of two coupled nonlinear integral constitutive equations with power-law memory kernels, or the direct simulation of typically  $10^5$  hopping SGR elements. In performing CFD with a fully tensorial stress, a corresponding number  $7N$  of degrees of freedom would be needed at each lattice site, as discussed further in Sec. VI. This should prove feasible for computing 2D flow fields on a small cluster. Even 3D flows should be feasible with further parallelization.

Finally, we reiterate that the assumption of a single value of  $l$  for any fixed  $E$  represents an approximation that, as discussed above, leads to typical factors of 2 between the quantitative predictions of the full and simplified SGR models, in the most nonlinear regimes of many protocols. Importantly, however, this assumption is in fact *exactly correct in linear rheology*. The simplified SGR model derived above is, therefore, predicted to give results that *exactly and quantitatively*

correspond to full SGR in any linear rheological protocol. Our numerical results will indeed confirm this.

With the exception of the right panel of Fig. 2, all the results presented will be in the model's glass phase,  $x < 1$ . Because the simplified model presented so far assumes a scalarized shear stress and contains no spatial information, all our numerical predictions will pertain to a homogeneous simple shear flow. In many of the protocols considered, however, shear bands would be expected to arise in any model that allowed heterogeneous flows, as described in Sec. I. This would modify the rheological signals to some extent compared with those computed below within the assumption of a homogeneous flow.

## V. RHEOLOGICAL PREDICTIONS OF THE SIMPLIFIED SGR MODEL

We now present our numerical results for the predictions of the simplified SGR model in homogeneous simple shear flow. We start with linear rheology in Sec. V A, before turning to address nonlinear flows. For any protocol in which the sample age explicitly features, we model the sample preparation at time  $t = 0$  via a sudden quench from an infinite initial noise temperature to a final noise temperature, usually (as just noted) in the glass phase,  $x < 1$ . This gives an initial distribution of trap depths  $G(E, t = 0) = \rho(E)$ . We further assume all local strains and stresses to be zero in this initial state, corresponding to an initially well relaxed sample. We then age the sample undisturbed for a time  $t_w$ , before imposing a strain or stress according to the protocol in question.

The aim of this work is not to undertake direct fitting of the model's predictions against any particular set of experimental data; nor yet exhaustively to review the available data for each protocol that follows. Nonetheless, we pause before

presenting our results to collect a few experimental references in which data qualitatively according with the key features of several of the figures that follow can be found: Fig. 1 [24], Fig. 2 [20,111], Fig. 3 [20], Fig. 4 [34], Fig. 6 [63], Fig. 7 [34], Fig. 9 [42]. Indeed, Purnomo *et al.* [111] carried out a quantitative fitting of the SGR model to measured viscoelastic spectra.

### A. Linear rheology

#### 1. Stress relaxation after linear step shear strain

A standard rheological test consists of suddenly straining a previously undeformed material by an amount  $\gamma_0$  at a time  $t_w$ . The shear strain is accordingly  $\gamma(t) = \gamma_0 \Theta(t - t_w)$ , where  $\Theta$  is the Heaviside function. The shear stress response can be written generally as

$$\sigma(t) = \gamma_0 G_{\text{step}}(t - t_w, t_w; \gamma_0). \quad (5.1)$$

In the limit of linear response,  $\gamma_0 \rightarrow 0$ , the  $\gamma_0$  dependence disappears from the stress relaxation function,  $G_{\text{step}}$ .

The left panel of Fig. 1 shows results for  $G_{\text{step}}(t - t_w, t_w)$  in this linear regime, computed within the full SGR model, for several sample ages  $t_w$  at a fixed noise temperature in the glass phase. As can be seen, the model predicts slow power law stress relaxation. It furthermore captures rheological aging, in which this stress relaxation takes place on a typical time scale that grows as the age of the sample  $t_w$ . This gives the observed collapse of the data for different values of  $t_w$ , as a function of the rescaled time interval,  $(t - t_w)/t_w$ .

Corresponding results for the simplified SGR model are shown in the right panel of Fig. 1, for matched parameter values. Excellent agreement is obtained between the full and simplified models, consistent with our above statement that the assumption made in moving from the full to the

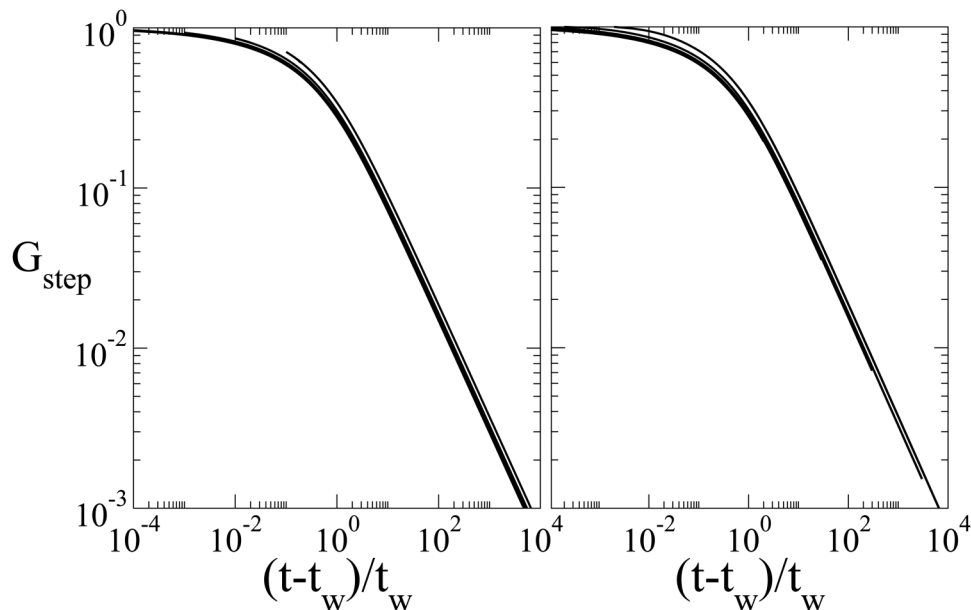


**FIG. 1.** Stress decay following a small amplitude step strain imposed at a waiting time  $t_w$ . Left: Results obtained within the full SGR model, by solving the integral constitutive equation of [16]. Right: Simplified SGR model. In both cases, the effective temperature  $x = 0.7$ , imposed shear strain  $\gamma_0 = 0.001$ , initial sample ages  $t_w = 10^2, 10^3, 10^4, 10^5, 10^6$ . In the simplified SGR model,  $E_{\text{max}} = 24.0$ ,  $N = 32$ , numerical time step  $dt = 0.1$ .

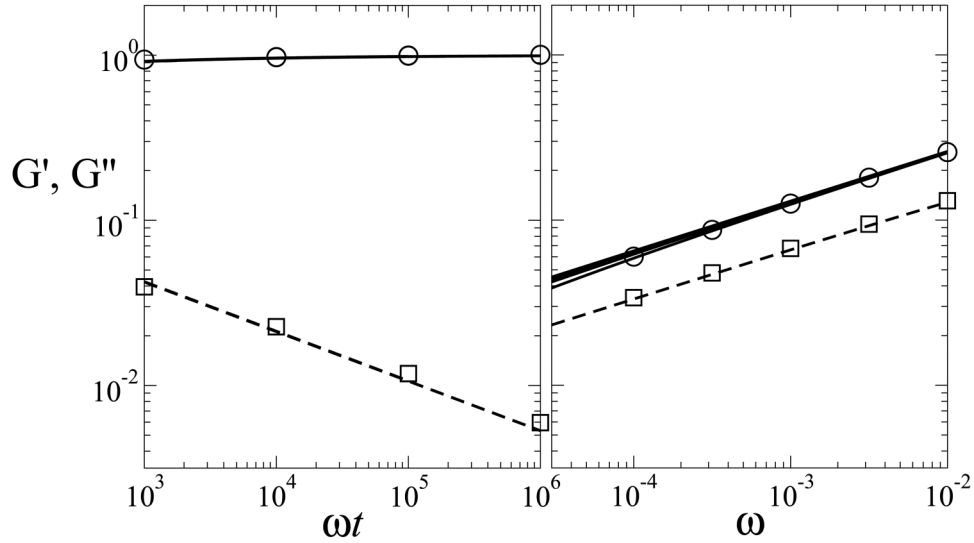


**FIG. 2.** Viscoelastic spectra of the full SGR model obtained by solving the integral constitutive equation of [16] (solid lines:  $G'$ , dashed lines:  $G''$ ) and simplified SGR model (circles:  $G'$ , squares:  $G''$ ). Left: for an effective temperature  $x = 0.7$ , as a function of frequency scaled by system's age,  $\omega t$ . Right: for an effective temperature  $x = 1.3$ , as a function of bare frequency  $\omega$ . Sample age  $t = 10^7$ . In the simplified SGR model,  $E_{\max} = 24.0$ ,  $N = 64$ ,  $dt = 0.01$ .

simplified model is exactly correct in the linear rheological regime.

## 2. Viscoelastic spectra

We now consider the viscoelastic spectra that characterize a material's stress response to a small amplitude oscillatory shear strain. As discussed in [15], the definition of viscoelastic spectra in an aging material needs some care because the time-translational invariance (TTI) that is usually implicitly assumed in defining these spectra breaks down as a consequence of aging.

Consider an experiment in which a sample is freshly prepared at time  $t = 0$  then allowed to age undisturbed to a time  $t_s$ . A small amplitude oscillatory shear strain of amplitude  $\gamma_0$  is started at this time  $t_s$  and maintained up to a later time  $t$ .

For such a protocol, one can unambiguously define a time-dependent viscoelastic spectrum,

$$G^*(\omega, t, t_s) = i\omega \int_{t_s}^t dt' e^{-i\omega(t-t')} G_{\text{step}}(t-t', t') + e^{-i\omega(t-t_s)} G_{\text{step}}(t-t_s, t_s), \quad (5.2)$$

where  $G_{\text{step}}(t-t', t')$  is the (non-TTI) stress relaxation function defined in Eq. (5.1), in the limit  $\gamma_0 \rightarrow 0$ . In 15, it was shown that the dependence of  $G^*$  on  $t_s$  becomes negligible in full SGR once many cycles have been performed,  $\omega(t-t_s) \gg 1$ , giving  $G^*(\omega, t, t_s) \rightarrow G^*(\omega, t)$ . Although intuitively reasonable, this simplification is not in fact guaranteed upfront in a glassy material with long term memory. Nonetheless, we now adopt  $G^*(\omega, t)$  as a working definition

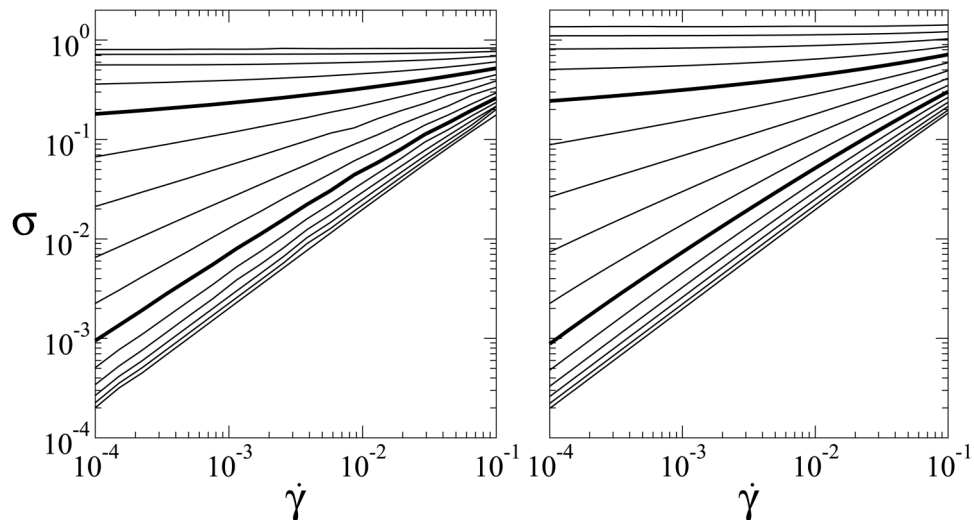


**FIG. 3.** Steady state flow curves. Left: full SGR model, obtained by solving the integral constitutive equation of 16. Right: simplified SGR model. In both cases, effective temperature values  $x = 0.2, 0.4, 0.6, \dots, 3.0$  (curves downward), with curves for  $x = 1.0$  and  $x = 2.0$  shown in bold. In the simplified SGR model,  $E_{\max} = 18.0$  and  $N = 32$ .

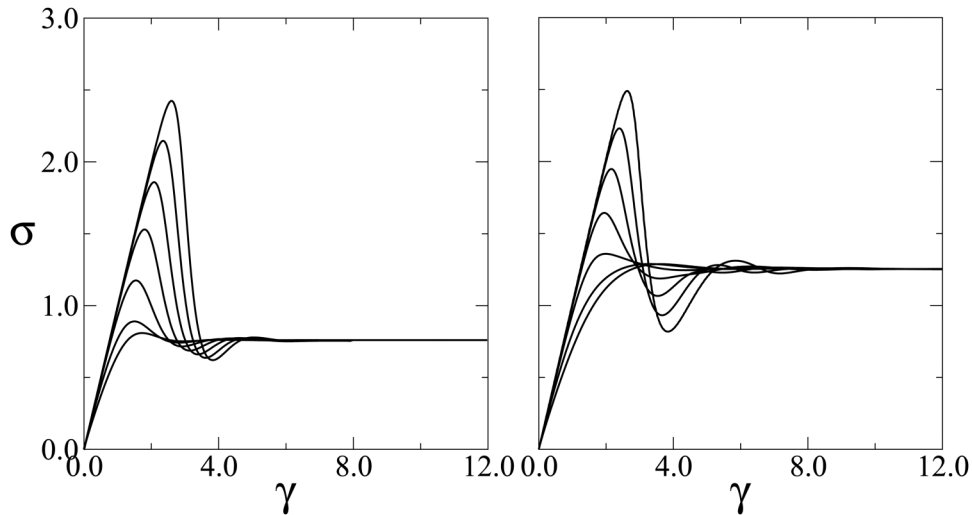


**FIG. 4.** Shear startup following the imposition of a step shear rate. Left: full SGR model obtained by solving the integral constitutive equation of [16]. Right: simplified SGR model. In both cases, effective temperature  $x = 0.3$ , imposed shear rate  $\dot{\gamma}_0 = 0.001$ , and initial sample ages  $t_w = 10^2, 10^3, 10^4, 10^5, 10^6, 10^7, 10^8$  (peak values upward). In the simplified SGR model,  $E_{\max} = 12.0$ ,  $N = 32$ ,  $dt = 0.03$ .

of the time-dependent viscoelastic spectrum for an aging material. Note, therefore, that the current time  $t$  plays the role of the sample age in this protocol, not the time  $t_s$ , now forgotten, at which the oscillatory shearing commenced.

Results for the real and imaginary parts of  $G^*(\omega, t)$ ,  $G'(\omega, t)$  and  $G''(\omega, t)$ , are shown for the full SGR model by the solid and dashed lines, respectively, in Fig. 2. The left panel shows results for a fixed sample age  $t$  at a noise temperature in the glass phase. The right panel shows results above the glass transition temperature. The spectra show a broad power-law dependence on frequency, consistent with the model's underlying spectrum of relaxation time scales. Corresponding results for the simplified SGR model are shown by symbols in the same figure. Excellent agreement with the full SGR model again substantiates our claim that the simplified model exactly agrees with the full model in the linear rheological regime.

## B. Nonlinear steady state flow curves

Having discussed the linear rheological regime, in which the full and simplified models exactly coincide, we now address nonlinear flows. We start by considering the steady state relationship between the shear stress and shear rate, as encoded in the flow curve,  $\sigma(\dot{\gamma})$ . Results for this quantity computed in the full SGR model are shown in the left panel of Fig. 3. For high noise temperatures,  $x > 2$ , the model displays Newtonian flow response in which  $\sigma \sim \dot{\gamma}$ . For intermediate noise temperatures,  $1 < x < 2$ , it shows power-law fluid behavior in which  $\sigma \sim \dot{\gamma}^{x-1}$ . For noise temperature in the glass phase,  $x < 1$ , the flow curve displays a yield stress  $\sigma_y(x)$  such that  $\sigma(\dot{\gamma}) - \sigma_y(x) \sim \dot{\gamma}^{1-x}$ . The yield stress  $\sigma_y$  shows a linear onset with  $x_g - x$  below the glass point.

Corresponding results computed within the simplified SGR model are shown in the right panel of the same figure. All the same quantitative features as in the full SGR model are preserved but with qualitative differences of about a

factor of 2 between the full and simplified models in the most strongly linear flows, i.e., in the glass phase.

## C. Dynamical nonlinear rheology: Imposed strain

### 1. Shear startup from rest

Consider now a startup experiment in which a shear of rate  $\dot{\gamma}_0$  is suddenly switched on at time  $t_w$ , with the shear rate held constant thereafter. We thus have  $\dot{\gamma}(t) = \dot{\gamma}_0 \Theta(t - t_w)$ , where  $\Theta$  is the Heaviside function.

The left panel of Fig. 4 shows results for the stress response as a function of accumulating strain,  $\gamma(t) = \dot{\gamma}_0(t - t_w)$ , computed in the glass phase of the full SGR model. At early time intervals, for which the accumulated strain is modest, the model shows an elastic solidlike response in which the stress increases linearly with strain,  $\sigma(t) = \gamma(t)$ , consistent with elements being in deep enough traps that their plastic relaxation is initially negligible. By contrast, in the limit of long times  $t \rightarrow \infty$  and large strains  $\gamma \rightarrow \infty$ , the sample flows in a liquidlike way, with the stress assuming a steady state value prescribed by the flow curve  $\sigma(\dot{\gamma}_0)$  described in Subsection V B. These early time solidlike and late-time liquidlike responses accordingly show no dependence on the age of the sample before the shearing commenced. In contrast, at intermediate strains, the stress overshoots its final steady state value, and the size of this overshoot shows a strong dependence on the sample age,  $t_w$ .

The right panel of Fig. 4 shows corresponding results computed within the simplified SGR model for matched parameter values. All the qualitative features are preserved in moving from the full to simplified SGR model and with only modest quantitative differences.

So far, we have seen that the simplified SGR model exactly reproduces the predictions of the full model in the regime of linear rheology. We have further shown that it reproduces the full model's qualitative behavior in the nonlinear steady state flow curve and in nonlinear shear startup with modest quantitative differences. Having thus developed

some confidence in the simplified SGR model, we now proceed to present some new rheological predictions within the simplified model that have not, to the author's knowledge, been previously computed within full SGR.

## 2. Shear rate jumps

Having discussed in Subsection V C 1, shear startup from an initial rest state,  $\dot{\gamma} = 0$ , to a shear rate  $\dot{\gamma}_0$ , we turn now to consider a protocol in which a sample is sheared at some initial rate  $\dot{\gamma}_1$  until it attains a steady flowing state and is then subject at some time  $t = 0$  to a shear rate jump to a final value  $\dot{\gamma}_2$ . To the author's knowledge, such a protocol has not previously been studied in the full SGR model. All the results presented here are computed within the simplified model.

In the left panel of Fig. 5, we show results for the time-dependent stress response  $\sigma(t)$  in several different upward strain rate jumps,  $\dot{\gamma}_2 > \dot{\gamma}_1$ . In each case, the stress starts at early times at its value as prescribed by the steady state flow curve,  $\sigma(\dot{\gamma}_1)$ , and tends at late times to a different value that is also prescribed by the steady state flow curve,  $\sigma(\dot{\gamma}_2)$ . (Because the flow curve is a rather flat function of shear rate for  $\dot{\gamma} \ll 1$  in the glass phase,  $x < 1$ , these initial and final values,  $\sigma(\dot{\gamma}_1)$  and  $\sigma(\dot{\gamma}_2)$ , are rather similar.)

Between these short- and long-time asymptotes, the stress displays an overshoot that depends on both  $\dot{\gamma}_1$  and  $\dot{\gamma}_2$ . The time at which the overshoot occurs appears to scale roughly as  $t \sim \dot{\gamma}_2^{-1}$ , to within logarithmic corrections set by  $\dot{\gamma}_1$ . The stress overshoot accordingly happens when the accumulated strain approaches a value  $O(1)$  (to within logarithmic corrections), consistent with elements then being pulled out of their traps by the imposed strain. The height of the overshoot is set by  $\dot{\gamma}_2/\dot{\gamma}_1$ .

The right panel of Fig. 5 shows counterpart results for downward strain rate jumps,  $\dot{\gamma}_2 < \dot{\gamma}_1$ . In this case, the stress signal shows an undershoot in between its initial and final

steady state values. The time at which this undershoot occurs increases with decreasing  $\dot{\gamma}_2$ , and its height is set by  $\dot{\gamma}_2/\dot{\gamma}_1$ .

## 3. Flow curve sweeps

Consider now a protocol in which a sample is presheared to a steady flowing state by executing  $\gamma_{\text{preshear}}$  strain units at a high shear rate  $\dot{\gamma}_{\text{max}}$ . The strain rate is then stepped downward in  $N_{\text{sweep}}$  logarithmic increments to a low strain rate  $\dot{\gamma}_{\text{min}}$ , waiting a time  $\Delta t$  at each strain rate value before further reducing the strain rate by a constant factor  $(\dot{\gamma}_{\text{max}}/\dot{\gamma}_{\text{min}})^{1/N_{\text{sweep}}}$ . Once  $\dot{\gamma}_{\text{min}}$  is attained the sweep is reversed, with the strain rate stepped upward through the same  $N_{\text{sweep}}$  values of strain rate, spending the same time  $\Delta t$  at each strain rate.

Figure 6 shows results for the stress obtained by the final time for each strain rate value, plotted as a function of that strain rate, for two different values of  $\Delta t$ . In each case, the black symbols denote the initial down-sweep and the red symbols the later up-sweep. These curves show all the same features as in the full SGR model [63], which can be summarized as follows.

Notable hysteresis is clearly evident between the down- and up-sweeps. Consider first the down-sweep. For strain rates higher than about  $10^{-2}$ , the stress lies on the steady state flow curve, which has a slight upward curvature as a function of  $\dot{\gamma}$ . At lower strain rates, the stress falls away from the steady state flow curve. This occurs because the system cannot age into deeper traps quickly enough to keep pace with the ever decreasing strain rate. Accordingly, the sample remains in a more fluidlike state than it would be at a true steady state for any imposed strain rate. The viscosity and shear stress, therefore, remain low compared with the values they would assume on the true steady state flow curve.

Once the strain rate reaches  $\dot{\gamma}_{\text{min}} = 10^{-6}$ , the up-sweep is commenced. During this up-sweep, the stress initially (i.e., at low strain rates) lies below that seen during the down-sweep.

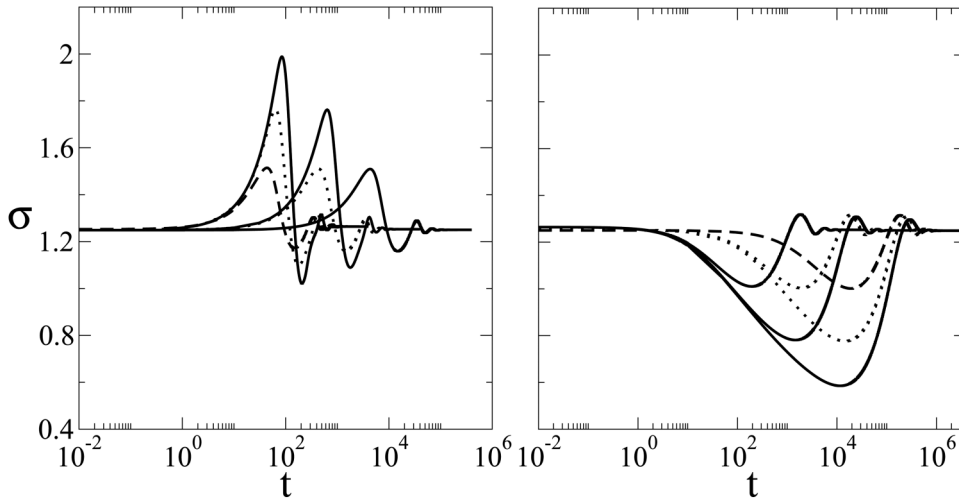


**FIG. 5.** Stress evolution following a shear rate jump in the simplified SGR model. In each run, the system is first evolved to steady state at an initial shear rate  $\dot{\gamma}_1$ . Then, at a time defined to be  $t = 0$ , the shear rate is jumped either up or down to  $\dot{\gamma}_2$  and the stress is plotted as a function of the time  $t$  since that jump. Left: upward strain rate jumps. Solid lines:  $\dot{\gamma}_1 = 10^{-5}$  with  $\dot{\gamma}_2 = 10^{-4}, 10^{-3}, 10^{-2}$ . Dotted lines:  $\dot{\gamma}_1 = 10^{-4}$  with  $\dot{\gamma}_2 = 10^{-3}, 10^{-2}$ . Dashed line:  $\dot{\gamma}_1 = 10^{-3}$  with  $\dot{\gamma}_2 = 10^{-2}$ . At any fixed  $\dot{\gamma}_1$ , times of stress peak move right with decreasing  $\dot{\gamma}_2$ . Right: downward strain rate jumps. Solid lines:  $\dot{\gamma}_1 = 10^{-2}$  with  $\dot{\gamma}_2 = 10^{-3}, 10^{-4}, 10^{-5}$ . Dotted lines:  $\dot{\gamma}_1 = 10^{-3}$  with  $\dot{\gamma}_2 = 10^{-4}, 10^{-5}$ . Dashed line:  $\dot{\gamma}_1 = 10^{-4}$  with  $\dot{\gamma}_2 = 10^{-5}$ . At any fixed  $\dot{\gamma}_1$ , times of stress dip move rightward with decreasing  $\dot{\gamma}_2$ .  $x = 0.3$ ,  $dt = 0.01$ ,  $E_{\text{max}} = 12.0$ ,  $N = 32$ .

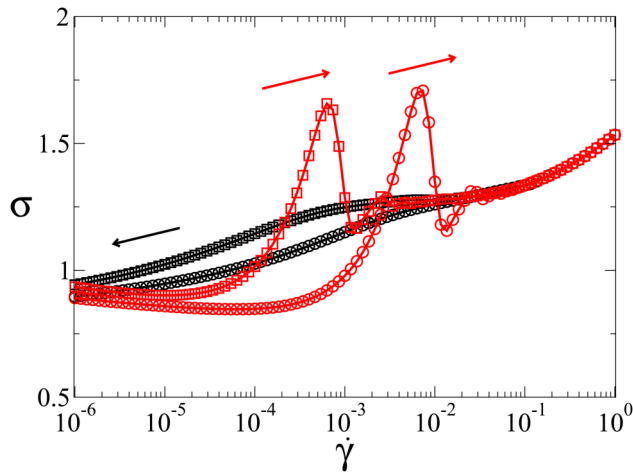


**FIG. 6.** Rheological hysteresis in the flow curve sweeps in the simplified SGR model. Two separate sweeps are shown. In each, the system is first sheared to steady state by executing  $\gamma_{\text{preshear}} = 250$  strain units at a high shear rate  $\dot{\gamma}_{\text{max}} = 1.0$ . The strain rate is then stepped downward to a low strain rate  $\dot{\gamma}_{\text{min}} = 10^{-6}$ , waiting a time  $\Delta t$  at each strain rate value before reducing the strain rate by a constant factor  $(\dot{\gamma}_{\text{max}}/\dot{\gamma}_{\text{min}})^{1/N_{\text{sweep}}}$ . The strain rate is then stepped upward through the same  $N_{\text{sweep}}$  values of strain rate with the same time  $\Delta t$  spent at each shear rate.  $N_{\text{sweep}} = 90$ . Circles:  $\Delta t = 25.0$ . Squares:  $\Delta t = 250.0$ . Black symbols: down-sweep. Red symbols: up-sweep. Effective temperature  $x = 0.3$ .  $dt = 0.01$ ,  $E_{\text{max}} = 12.0$ ,  $N = 32$ .

Indeed, it even decreases with increasing  $\dot{\gamma}$ . This is because the stress response of the SGR model is intrinsically viscoelastic. Accordingly, the sample retains some memory of the stress it had accumulated at the earlier high values of strain rate during the down-sweep, which is still slowly relaxing even as the shear rate increases again during the up-sweep.

This regime of declining stress ends with a steep upturn in the stress as the strain rate increases yet further. The up-sweep stress then rises above its down-sweep counterpart and indeed overshoots its flow-curve value, before finally declining to meet the steady state flow curve at the highest strain rates. This overshoot is the counterpart to that seen in shear startup in Fig. 4 and other upward shear rate jumps in Fig. 5. The shear rate at which the overshoot occurs is seen to scale as  $1/\Delta t$ . Indeed, all the features just described shift a decade to the left between the curves for  $\Delta t = 25.0$  and  $\Delta t = 250.0$ .

#### 4. Large-amplitude oscillatory shear

Let us consider now a protocol in which a sample is freshly prepared at an initial time  $t = 0$ , then left to age undisturbed to a time  $t_w$  before an oscillatory shear strain is commenced,  $\gamma(t) = \gamma_0 \sin(\omega t)$ . We present here results obtained within the simplified SGR model. LAOS has been previously studied in the full SGR model (extended to allow shear banding) in [59] and [60].

For values of  $\gamma_0$  in the nonlinear regime, we find that the system attains after many strain cycles a state in which the stress response is invariant under cycle-to-cycle translations,  $t \rightarrow t + 2\pi/\omega$ . For small  $\gamma_0$ , the sample instead continues to age slightly from cycle to cycle, as seen in the viscoelastic spectra of Fig. 2, left. Figure 7 shows parametric so-called LB plots of the stress  $\sigma(t)$  as a function of strain  $\gamma(t)$  for the

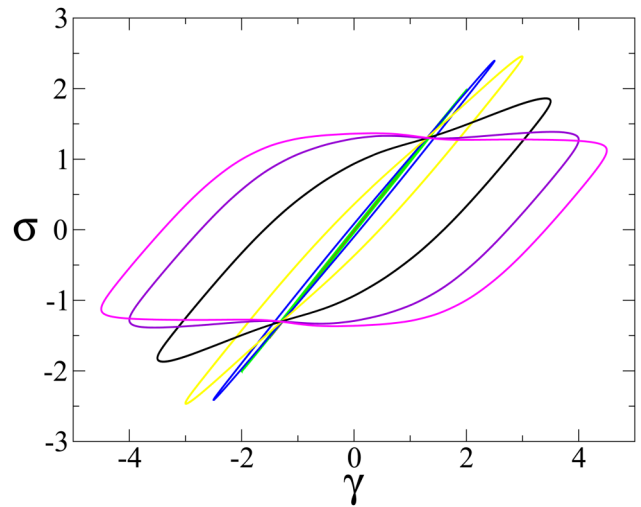


**FIG. 7.** Lissajous–Bowditch figures showing a parametric plot of stress  $\sigma(t)$  against strain  $\gamma(t)$  during LAOS in the simplified SGR model. Effective temperature  $x = 0.3$  and initial sample age  $t_w = 10$ . The imposed strain  $\gamma(t) = \gamma_0 \sin(\omega t)$  with  $\omega = 0.01$  and  $\gamma_0 = 1.0, 1.5, 2.0, \dots, 4.5$  (curves outward). For each value of  $\gamma_0$ , data are shown for the 99th and 100th cycles, with the data for these two cycles not being discernible from each other by eye.  $dt = 0.005$ ,  $E_{\text{max}} = 12.0$ ,  $N = 32$ .

99th and 100th cycles, indeed with no discernible difference in the stress response between these two cycles. Curves are shown for several values of the imposed strain amplitude,  $\gamma_0$ , for a fixed frequency  $\omega$ . The value of  $\gamma_0$  in each case can be simply read off from the maximum value of  $\gamma(t)$  attained during the cycle.

For low values of  $\gamma_0$ , each LB curve takes the form of a highly elongated, almost needlelike ellipse, oriented so as to have a slope  $\sigma'(\gamma) \approx 1$  over much of the cycle (except, obviously, at the turning points of maximum and minimum strain). This is consistent with the SGR model showing rather elastic behavior at stresses below the yield stress, with modulus  $k = 1$  in our units. For the intermediate strain amplitudes explored,  $\gamma_0 = 3.0$  and  $\gamma_0 = 3.5$ , the LB curves instead adopt a characteristic diamond shape, again with a slope  $\approx 1$  for stresses below the yield stress, but now with a reduced slope for higher stresses. At the highest strain amplitudes  $\gamma_0$ , the LB curves likewise show a slope  $\approx 1$  for stresses below the yield stress but are much flatter above yield.

The same progression in the shapes of the LB curves with increasing strain amplitude  $\gamma_0$  is also seen in the full SGR model. Curves such as these have been discussed in detail in the LAOS literature for yield stress fluids in terms of a sequence of physical processes, with elastic caging at low stresses and yielding at higher stresses [112].

In Ref. [56], experimental data for a Carbopol gel in a LAOS (albeit in that work for LAOStress rather than LAOStrain) was compared with the so-called elastic Herschel–Bulkley (EHB) model. That model is constructed to give a stress linear in strain below the yield stress, and a Herschel–Bulkley relationship between stress and strain rate above yield (as in the steady state flow curve of the SGR model). The EHB model fails to capture the diamond-shaped LB curves seen experimentally in Ref. [56] and reproduced here for intermediate values of strain amplitudes in SGR.

In particular, the part of these diamond-shaped LB curves above yield shows a hardening *compared with EHB*. (Care is warranted with nomenclature here, because this part of the curve represents a *softening* relative to the elastic regime below yield.)

Motivated by this observed hardening relative to EHB, many recent attempts to build constitutive models of elastoplastic rheology have incorporated the concept of “kinematic hardening.” This is typically discussed as modeling the movement of the center of a material’s yield surface and is captured by including in the constitutive model equations an additional variable termed the “back-stress.” Attempts to justify this back-stress in terms of underlying mesoscopic physics, however, remain largely unsatisfactory to date.

A pleasing feature of SGR is that it naturally captures these diamond-shaped LB curves (and many other features of elastoplastic rheology besides) without recourse to the notion of a back-stress. How any effective back-stress emerges from the SGR model remains an interesting question. Feasibly, it could represent one of the next higher moments of the local strain distribution, besides the average strain encoded in the first moment.

### 5. Strain cycling: Bauschinger effect

In 1886, Bauschinger reported an effective reduction in the tensile yield stress of a polycrystalline metal following a tensile prestrain in the opposite direction [113]. The effect has since also been discussed in the context of shear deformations. We shall now explore this Bauschinger effect within the simplified SGR model. To do so, let us consider a protocol in which a sample is freshly prepared at time  $t = 0$ , then left to age undisturbed before a forward shear rate  $\dot{\gamma}$  is applied up to a forward strain  $\gamma_0$ . The strain is then reversed at an equal and opposite applied shear rate,  $-\dot{\gamma}$ , up to a final strain of  $-10$  units.

Figure 8 shows the predictions of the simplified SGR model in this protocol. The initial sample age  $t_w$  increases by

a factor 10 between each successive panel from left to right across the figure. In each panel, results are shown for several values of the total forward strain  $\gamma_0$  applied before the strain direction is reversed.

During the initial forward straining phase SGR predicts a stress overshoot. Indeed, we have already discussed this in the context of a simple forward shear startup experiment. Recall Fig. 4. The associated yield stress and strain increase with increasing sample age  $t_w$  across the panels of Fig. 8 from left to right. The degree to which this stress overshoot and subsequent stress decline are explored, for any  $t_w$ , increases with increasing  $\gamma_0$ . For values of  $\gamma_0$  large enough to give significant yielding in this forward direction, a reduced yield stress is then observed during the subsequent backward straining. This corresponds to a Bauschinger effect (asymmetry between the initial forward and subsequent backward yield stress), the size of which increases with increasing age of the sample  $t_w$  before the first, forward shear commenced.

### D. Dynamical nonlinear rheology: Imposed stress

So far, we have discussed the predictions of the simplified SGR model for rheological protocols in which the shear strain is imposed as a function of time. We turn finally to a common stress-imposed protocol. In particular, we consider a sample that is freshly prepared at time  $t = 0$  and left to age undisturbed up to a time  $t_w$ , when a step shear stress of amplitude  $\sigma_0$  is suddenly applied. The imposed stress is accordingly  $\sigma(t) = \sigma_0 \Theta(t - t_w)$ , where  $\Theta$  is the Heaviside function.

The strain rate response as a function of time  $t - t_w$  is shown in Fig. 9 for a fixed value of the sample age  $t_w$  and several values of the imposed stress  $\sigma_0$  from below to above the yield stress  $\sigma_y$  (defined as the stress attained in the limit  $\dot{\gamma} \rightarrow 0$  of the steady state flow curve).

For the smallest imposed stress values shown, the shear rate decays as a function of time, and the corresponding

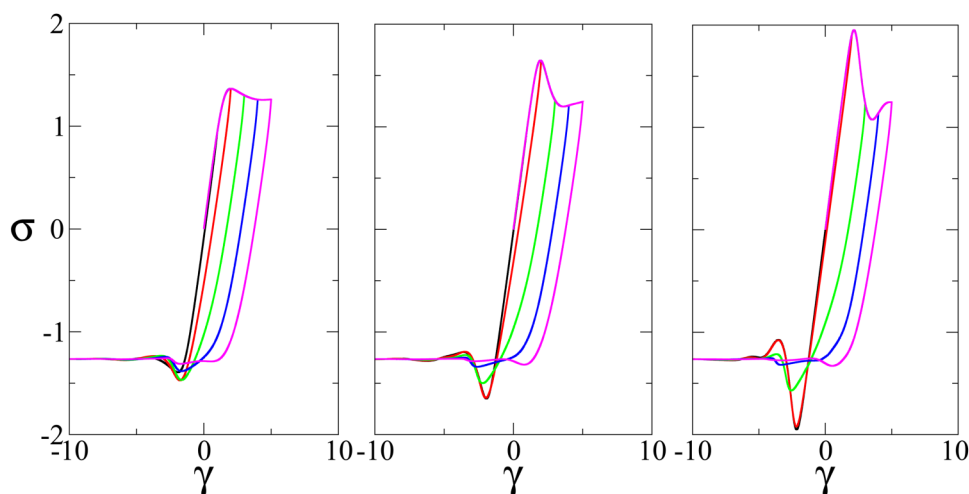


**FIG. 8.** Age-dependent Bauschinger effect in the simplified SGR model. Parametric plot of stress  $\sigma(t)$  against strain  $\gamma(t)$  in (first) a forward strain by  $\gamma_0$  strain units at a rate  $\dot{\gamma} = 0.01$  followed (second) by a reverse strain at a rate  $\dot{\gamma} = -0.01$  to a final strain of  $-10$  units. Effective temperature  $x = 0.3$ . Initial sample age before shearing commences: (left)  $t_w = 10^3$ , (middle)  $t_w = 10^4$ , and (right)  $t_w = 10^5$ . In each panel, the imposed forward strain  $\gamma_0 = 1.0, 2.0, 3.0, 4.0, 5.0$  (curves rightward).  $dt = 0.01$ ,  $E_{\max} = 12.0$ ,  $N = 32$ .

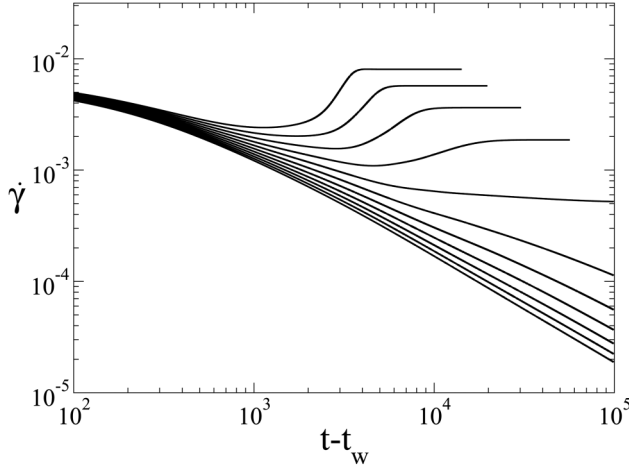


**FIG. 9.** Creep and (for imposed stress values  $\sigma_0 > \sigma_y$ ) yielding following the imposition of a step stress of amplitude  $\sigma_0$  at time  $t_w$  in the simplified SGR model. Effective temperature  $x = 0.3$ , initial sample age  $t_w = 10^3$ . Imposed stress values, scaled by the yield stress, are  $\sigma_0/\sigma_y = 0.990, 0.992, \dots, 1.010$  (curves upward).  $dt = 0.01$ ,  $E_{\max} = 8.0$ ,  $N = 64$ .

strain response increases sublinearly. In this way, the material creeps ever forward, but at an ever declining shear rate, never attaining a flowing state of constant nonzero  $\dot{\gamma}$ . For the imposed stresses just above  $\sigma_y$ , the sample initially displays a window of sublinear creep in which the shear rate progressively decreases, much as it would for an imposed stress below yield. In marked contrast, however, at later times the sample yields and the shear rate suddenly increases to attain its value as prescribed by the steady state flow curve  $\sigma(\dot{\gamma})$ . The same behavior was reported (in the format of strain versus time) in the full SGR model in [15].

This ability of the SGR model to capture power creep followed by fluidization and yielding following the imposition of a step shear stress just above the yield stress should be particularly noted. Reports of such behavior in other constitutive models of elastoplastic fluids (at least in those that have monotonic underlying constitutive curves  $\sigma(\dot{\gamma})$ , precluding steady state shear banding) are rare [114]: it appears difficult to capture this complicated behavior in a simple constitutive model with just a small number of dynamical variables.

## VI. POSSIBLE TENSORIAL GENERALIZATION

So far, we have presented a simplified SGR model with only a scalarized shear stress. In order to perform CFD, one needs a constitutive model with a fully tensorial stress. We offer finally one possible choice for such a model, following here the simplest path to tensorializing the scalar model discussed above and leaving other more sophisticated generalizations for future work.

We define the stress carried in wells of depth  $E$  as

$$\Sigma(E, t) = G(E, t)I(E, t), \quad (6.1)$$

where we have defined a new tensorial strain variable  $I$ . We

then write the evolution equations

$$\begin{aligned} \left(\frac{d}{dt} + \mathbf{v} \cdot \nabla\right) G(E, t) &= -\frac{G(E, t)}{\tau(E, I(E, t))} + \rho(E)Y(t), \\ \left(\frac{d}{dt} + \mathbf{v} \cdot \nabla\right) \Sigma(E, t) &= \Sigma(E, t) \cdot \mathbf{K} + \mathbf{K}^T \cdot \Sigma(E, t) \\ &\quad + 2G(E, t)\mathbf{D} - \frac{\Sigma(E, t)}{\tau(E, I(E, t))}. \end{aligned} \quad (6.2)$$

Here,  $\mathbf{K}$  is the velocity gradient tensor and  $\mathbf{D}$  its symmetric part. We then have the usual definition of the hopping rate,

$$Y(t) = \int dE \frac{G(E, t)}{\tau(E, I(E, t))}, \quad (6.3)$$

and the prior distribution,

$$\rho(E) = \exp(-E). \quad (6.4)$$

The time constant is now defined as

$$\tau(E, I) = \tau_0 \exp\left(\frac{E - I(I)}{x}\right), \quad (6.5)$$

in which  $I$  is a suitable invariant of the local strain tensor  $\mathbf{l}$ , for which we suggest  $I = \frac{1}{2}\mathbf{l}:\mathbf{l}$ . We note that the strain tensor,  $\mathbf{l}$ , is defined by the ratio of the stress tensor,  $\Sigma$ , and the modulus,  $G$ , via Eq. (6.1).

To compute the response of this tensorial model in homogeneous flow would require the evolution of  $7N$  time-differential equations: one at each  $N$  for  $G$  and six for each independent component of the symmetric tensor  $\Sigma$ , having again discretized  $E$  on a grid of  $N$  values. To perform CFD would require  $7N$  such variables at each lattice site, with three additional variables for the flow velocity vector.

## VII. CONCLUSIONS

In this work, we have introduced a simplified constitutive model for the elastoviscoplastic rheology of yield stress fluids, motivated by the widely used SGR model. We have demonstrated this simplified model to capture a wide array of observed rheological behaviors in both strain-imposed and stress-imposed flow protocols, in both the linear and nonlinear rheological regimes. Once suitable units of modulus, length, and time are chosen, the model has only one dimensionless parameter: the effective noise temperature,  $x$ .

The original SGR model on which this simplified model is based has been widely used in the literature. However, the computation within it of even homogeneous simple shear flows is considerably cumbersome, involving the solution of a PDE,  $\partial_t P(E, l, t) = \dots$ , or the solution of two coupled nonlinear integral equations, or the direct simulation of typically  $10^5$  hopping SGR elements.

In contrast, the computation of homogeneous simple shear flows within the simplified model requires the time evolution of only  $2N$  relatively simple differential equations, with values of  $N$  as low as 16 giving good results. This renders SGR much more readily accessible to anyone wishing to fit

its predictions to rheometric data. Whereas the original model was prohibitively costly for use in CFD to address flows in complicated geometries, or complicated flows arising due to spontaneous symmetry breaking instabilities even in simple geometries, the simplified model is now sufficiently simple for use in CFD, once suitably tensorialized. Indeed, work is currently in progress to benchmark its behavior in the canonical CFD geometries of 2D flow past a cylinder and 3D flow past a sphere.

## ACKNOWLEDGMENTS

The author thanks Andrew Clarke for discussions and Mike Cates, Gareth McKinley, and Ron Larson for feedback on the manuscript. Schlumberger Cambridge Research is acknowledged for funding.

## REFERENCES

- [1] Bonn, D., M. M. Denn, L. Berthier, T. Divoux, and S. Manneville, "Yield stress materials in soft condensed matter," *Rev. Mod. Phys.* **89**, 035005 (2017).
- [2] Coussot, P., "Slow flows of yield stress fluids: Yielding liquids or flowing solids?," *Rheol. Acta* **57**, 1–14 (2018).
- [3] Coussot, P., "Yield stress fluid flows: A review of experimental data," *J. Non-Newton. Fluid Mech.* **211**, 31–49 (2014).
- [4] Bonn, D., and M. M. Denn, "Yield stress fluids slowly yield to analysis," *Science* **324**, 1401–1402 (2009).
- [5] Coussot, P., "Rheophysics of pastes: A review of microscopic modeling approaches," *Soft Matter* **3**, 528–540 (2007).
- [6] Denn, M. M., and D. Bonn, "Issues in the flow of yield-stress liquids," *Rheol. Acta* **50**, 307–315 (2011).
- [7] Balmforth, N. J., I. A. Frigaard, and G. Ovarlez, "Yielding to stress: Recent developments in viscoplastic fluid mechanics," *Annu. Rev. Fluid Mech.* **46**, 121–146 (2014).
- [8] Moller, P. C., J. Mewis, and D. Bonn, "Yield stress and thixotropy: On the difficulty of measuring yield stresses in practice," *Soft Matter* **2**, 274–283 (2006).
- [9] Herschel, W., and R. Bulkley, "Consistency measurements of rubberbenzol solutions," *Kolloid-Zeitschrift* **39**, 291–300 (1926).
- [10] Bingham, E. C., *Fluidity and Plasticity* (McGraw-Hill, New York, 1922), Vol. 2.
- [11] Larson, R. G., and Y. Wei, "A review of thixotropy and its rheological modeling," *J. Rheol.* **63**, 477–501 (2019).
- [12] Ikeda, A., L. Berthier, and P. Sollich, "Unified study of glass and jamming rheology in soft particle systems," *Phys. Rev. Lett.* **109**, 018301 (2012).
- [13] Ikeda, A., L. Berthier, and P. Sollich, "Disentangling glass and jamming physics in the rheology of soft materials," *Soft Matter* **9**, 7669–7683 (2013).
- [14] Sollich, P., F. Lequeux, P. Hebraud, and M. Cates, "Rheology of soft glassy materials," *Phys. Rev. Lett.* **78**, 2020–2023 (1997).
- [15] Fielding, S., P. Sollich, and M. Cates, "Aging and rheology in soft materials," *J. Rheol.* **44**, 323–369 (2000).
- [16] Sollich, P., "Rheological constitutive equation for a model of soft glassy materials," *Phys. Rev. E* **58**, 738–759 (1998).
- [17] Mackley, M., R. Marshall, J. Smeulders, and F. Zhao, "The rheological characterization of polymeric and colloidal fluids," *Chem. Eng. Sci.* **49**, 2551–2565 (1994).
- [18] Ketz, R., R. K. Prud'homme, and W. Graessley, "Rheology of concentrated microgel solutions," *Rheol. Acta* **27**, 531–539 (1988).
- [19] Khan, S. A., C. A. Schnepper, and R. C. Armstrong, "Foam rheology: III. Measurement of shear flow properties," *J. Rheol.* **32**, 69–92 (1988).
- [20] Mason, T., J. Bibette, and D. Weitz, "Elasticity of compressed emulsions," *Phys. Rev. Lett.* **75**, 2051–2054 (1995).
- [21] Panizza, P., D. Roux, V. Vuillaume, C.-Y. Lu, and M. Cates, "Viscoelasticity of the onion phase," *Langmuir* **12**, 248–252 (1996).
- [22] Hoffmann, H., and A. Rauscher, "Aggregating systems with a yield stress value," *Colloid Polym. Sci.* **271**, 390–395 (1993).
- [23] Mason, T., and D. Weitz, "Linear viscoelasticity of colloidal hard sphere suspensions near the glass transition," *Phys. Rev. Lett.* **75**, 2770–2773 (1995).
- [24] Ramos, L., and L. Cipelletti, "Ultraslow dynamics and stress relaxation in the aging of a soft glassy system," *Phys. Rev. Lett.* **87**, 245503 (2001).
- [25] Batista, A. P., A. Raymundo, I. Sousa, J. Empis, and J. M. Franco, "Colored food emulsions—implications of pigment addition on the rheological behavior and microstructure," *Food Biophys.* **1**, 216–227 (2006).
- [26] Papenhuijzen, J., "The role of particle interactions in the rheology of dispersed systems," *Rheol. Acta* **11**, 73–88 (1972).
- [27] Divoux, T., D. Tamarii, C. Barentin, and S. Manneville, "Transient shear banding in a simple yield stress fluid," *Phys. Rev. Lett.* **104**, 208301 (2010).
- [28] Divoux, T., C. Barentin, and S. Manneville, "Stress overshoot in a simple yield stress fluid: An extensive study combining rheology and velocimetry," *Soft Matter* **7**, 9335–9349 (2011).
- [29] Martin, J. D., and Y. T. Hu, "Transient and steady-state shear banding in aging soft glassy materials," *Soft Matter* **8**, 6940–6949 (2012).
- [30] Gibaud, T., C. Barentin, and S. Manneville, "Influence of boundary conditions on yielding in a soft glassy material," *Phys. Rev. Lett.* **101**, 258302 (2008).
- [31] Kurokawa, A., V. Vidal, K. Kurita, T. Divoux, and S. Manneville, "Avalanche-like fluidization of a non-Brownian particle gel," *Soft Matter* **11**, 9026–9037 (2015).
- [32] Koumakis, N., and G. Petekidis, "Two step yielding in attractive colloids: Transition from gels to attractive glasses," *Soft Matter* **7**, 2456–2470 (2011).
- [33] Liddel, P. V., and D. V. Boger, "Yield stress measurements with the vane," *J. Non-Newton. Fluid Mech.* **63**(2–3), 235–261 (1996).
- [34] Dimitriou, C. J., and G. H. McKinley, "A comprehensive constitutive law for waxy crude oil: A thixotropic yield stress fluid," *Soft Matter* **10**, 6619–6644 (2014).
- [35] Divoux, T., C. Barentin, and S. Manneville, "From stress-induced fluidization processes to Herschel-Bulkley behaviour in simple yield stress fluids," *Soft Matter* **7**, 8409–8418 (2011).
- [36] Magnin, A., and J. M. Piau, "Cone-and-plate rheometry of yield stress fluids—Study of an aqueous gel," *J. Non-Newton. Fluid Mech.* **36**, 85–108 (1990).
- [37] Gibaud, T., D. Frelat, and S. Manneville, "Heterogeneous yielding dynamics in a colloidal gel," *Soft Matter* **6**, 3482–3488 (2010).
- [38] Grenard, V., T. Divoux, N. Taberlet, and S. Manneville, "Timescales in creep and yielding of attractive gels," *Soft Matter* **10**, 1555–1571 (2014).
- [39] Sprakel, J., S. B. Lindström, T. E. Kodger, and D. A. Weitz, "Stress enhancement in the delayed yielding of colloidal gels," *Phys. Rev. Lett.* **106**, 248303 (2011).
- [40] Bauer, T., J. Oberdisse, and L. Ramos, "Collective rearrangement at the onset of flow of a polycrystalline hexagonal columnar phase," *Phys. Rev. Lett.* **97**, 258303 (2006).

- [41] Sentjabrskaja, T., P. Chaudhuri, M. Hermes, W. C. K. Poon, J. Horbach, S. U. Egelhaaf, and M. Laurati, “Creep and flow of glasses: Strain response linked to the spatial distribution of dynamical heterogeneities,” *Sci. Rep.* **5**, 11884 (2015).
- [42] Siebenbürger, M., M. Ballauff, and T. Voigtmann, “Creep in colloidal glasses,” *Phys. Rev. Lett.* **108**, 255701 (2012).
- [43] Yoshimura, A. S., and R. K. Prud’homme, “Response of an elastic Bingham fluid to oscillatory shear,” *Rheol. Acta* **26**, 428–436 (1987).
- [44] Knaebel, A., M. Bellour, J.-P. Munch, V. Viasnoff, F. Lequeux, and J. L. Harden, “Aging behavior of laponite clay particle suspensions,” *Europhys. Lett.* **52**, 73–79 (2000).
- [45] Viasnoff, V., S. Jurine, and F. Lequeux, “How are colloidal suspensions that age rejuvenated by strain application?,” *Faraday Discuss.* **123**, 253–266 (2003).
- [46] Rouyer, F., S. Cohen-Addad, R. Höhler, P. Sollich, and S. M. Fielding, “The large amplitude oscillatory strain response of aqueous foam: Strain localization and full stress Fourier spectrum,” *Eur. Phys. J. E* **27**, 309–321 (2008).
- [47] Ewoldt, R. H., P. Winter, J. Maxey, and G. H. McKinley, “Large amplitude oscillatory shear of pseudoplastic and elastoviscoplastic materials,” *Rheol. Acta* **49**, 191–212 (2010).
- [48] Renou, F., J. Stellbrink, and G. Petekidis, “Yielding processes in a colloidal glass of soft star-like micelles under large amplitude oscillatory shear (LAOS),” *J. Rheol.* **54**, 1219–1242 (2010).
- [49] van der Vaart, K., Y. Rahmani, R. Zargar, Z. Hu, D. Bonn, and P. Schall, “Rheology of concentrated soft and hard-sphere suspensions,” *J. Rheol.* **57**, 1195–1209 (2013).
- [50] Koumakis, N., J. F. Brady, and G. Petekidis, “Complex oscillatory yielding of model hard-sphere glasses,” *Phys. Rev. Lett.* **110**, 178301 (2013).
- [51] Poulos, A. S., J. Stellbrink, and G. Petekidis, “Flow of concentrated solutions of starlike micelles under large-amplitude oscillatory shear,” *Rheol. Acta* **52**(8–9), 785–800 (2013).
- [52] Poulos, A. S., F. Renou, A. R. Jacob, N. Koumakis, and G. Petekidis, “Large amplitude oscillatory shear (LAOS) in model colloidal suspensions and glasses: Frequency dependence,” *Rheol. Acta* **54**, 715–724 (2015).
- [53] Cohen, I., B. Davidovitch, A. B. Schofield, M. P. Brenner, and D. A. Weitz, “Slip, yield, and bands in colloidal crystals under oscillatory shear,” *Phys. Rev. Lett.* **97**, 215502 (2006).
- [54] Perge, C., N. Taberlet, T. Gibaud, and S. Manneville, “Time dependence in large amplitude oscillatory shear: A rheo-ultrasonic study of fatigue dynamics in a colloidal gel,” *J. Rheol.* **58**, 1331–1357 (2014).
- [55] Guo, Y., W. Yu, Y. Xu, and C. Zhou, “Correlations between local flow mechanism and macroscopic rheology in concentrated suspensions under oscillatory shear,” *Soft Matter* **7**, 2433–2443 (2011).
- [56] Dimitriou, C. J., R. H. Ewoldt, and G. H. McKinley, “Describing and prescribing the constitutive response of yield stress fluids using large amplitude oscillatory shear stress (LAOS<sub>Stress</sub>),” *J. Rheol.* **57**, 27–70 (2013).
- [57] Gibaud, T., C. Perge, S. B. Lindstrom, N. Taberlet, and S. Manneville, “Multiple yielding processes in a colloidal gel under large amplitude oscillatory stress,” *Soft Matter* **12**, 1701–1712 (2016).
- [58] Park, J. D., and S. A. Rogers, “The transient behavior of soft glassy materials far from equilibrium,” *J. Rheol.* **62**, 869–888 (2018).
- [59] Radhakrishnan, R., and S. M. Fielding, “Shear banding in large amplitude oscillatory shear (LAOS<sub>Strain</sub> and LAOS<sub>Stress</sub>) of soft glassy materials,” *J. Rheol.* **62**, 559–576 (2018).
- [60] Radhakrishnan, R., and S. M. Fielding, “Shear banding of soft glassy materials in large amplitude oscillatory shear,” *Phys. Rev. Lett.* **117**, 188001 (2016).
- [61] Bannantine, J., J. Comer, and J. Handrock, *Fundamentals of Metal Fatigue Analysis* (Prentice Hall, Englewood Cliffs, NJ, 1990), p. 286.
- [62] Karmakar, S., E. Lerner, and I. Procaccia, “Plasticity-induced anisotropy in amorphous solids: The Bauschinger effect,” *Phys. Rev. E* **82**(2 Pt 2), 026104 (2010).
- [63] Radhakrishnan, R., T. Divoux, S. Manneville, and S. M. Fielding, “Understanding rheological hysteresis in soft glassy materials,” *Soft Matter* **13**, 1834–1852 (2017).
- [64] Divoux, T., V. Grenard, and S. Manneville, “Rheological hysteresis in soft glassy materials,” *Phys. Rev. Lett.* **110**, 018304 (2013).
- [65] Colombo, J., and E. Del Gado, “Stress localization, stiffening, and yielding in a model colloidal gel,” *J. Rheol.* **58**, 1089–1116 (2014).
- [66] Shrivastav, G. P., P. Chaudhuri, and J. Horbach, “Yielding of glass under shear: A directed percolation transition precedes shear-band formation,” *Phys. Rev. E* **94**, 042605 (2016).
- [67] Shi, Y., M. B. Katz, H. Li, and M. L. Falk, “Evaluation of the disorder temperature and free-volume formalisms via simulations of shear banding in amorphous solids,” *Phys. Rev. Lett.* **98**, 185505 (2007).
- [68] Varnik, F., L. Bocquet, and J. L. Barrat, “A study of the static yield stress in a binary Lennard-Jones glass,” *J. Chem. Phys.* **120**, 2788–2801 (2004).
- [69] Kabla, A., J. Scheibert, and G. Debregeas, “Quasi-static rheology of foams. Part 2. Continuous shear flow,” *J. Fluid Mech.* **587**, 45–72 (2007).
- [70] Barry, J. D., D. Weaire, and S. Hutzler, “Shear localisation with 2D viscous froth and its relation to the continuum model,” *Rheol. Acta* **49**(6, SI), 687–698 (2010).
- [71] Moorcroft, R. L., M. E. Cates, and S. M. Fielding, “Age-dependent transient shear banding in soft glasses,” *Phys. Rev. Lett.* **106**, 055502 (2011).
- [72] Fielding, S. M., “Shear banding in soft glassy materials,” *Rep. Prog. Phys.* **77**, 102601 (2014).
- [73] Lehtinen, A., A. Puisto, X. Illa, M. Mohtaschemi, and M. J. Alava, “Transient shear banding in viscoelastic Maxwell fluids,” *Soft Matter* **9**, 8041–8049 (2013).
- [74] Manning, M. L., J. S. Langer, and J. M. Carlson, “Strain localization in a shear transformation zone model for amorphous solids,” *Phys. Rev. E* **76**, 056106 (2007).
- [75] Manning, M. L., E. G. Daub, J. S. Langer, and J. M. Carlson, “Rate-dependent shear bands in a shear-transformation-zone model of amorphous solids,” *Phys. Rev. E* **79**, 016110 (2009).
- [76] Jagla, E. A., “Shear band dynamics from a mesoscopic modeling of plasticity,” *J. Stat. Mech. Theory E* **2010**, P12025 (2010).
- [77] Chaudhuri, P., and J. Horbach, “Onset of flow in a confined colloidal glass under an imposed shear stress,” *Phys. Rev. E* **88**, 040301 (2013).
- [78] Moorcroft, R. L., and S. M. Fielding, “Criteria for shear banding in time-dependent flows of complex fluids,” *Phys. Rev. Lett.* **110**, 086001 (2013).
- [79] Coussot, P., J. S. Raynaud, F. Bertrand, P. Moucheron, J. P. Guilbaud, H. T. Huynh, S. Jarny, and D. Lesueur, “Coexistence of liquid and solid phases in flowing soft-glassy materials,” *Phys. Rev. Lett.* **88**, 218301 (2002).
- [80] Ragouilliaux, A., B. Herzhaft, F. Bertrand, and P. Coussot, “Flow instability and shear localization in a drilling mud,” *Rheol. Acta* **46**, 261–271 (2006).
- [81] Brader, J. M., M. E. Cates, and M. Fuchs, “First-principles constitutive equation for suspension rheology,” *Phys. Rev. Lett.* **101**, 138301 (2008).
- [82] Amann, C. P., M. Siebenbuerger, M. Krueger, F. Weysser, M. Ballauff, and M. Fuchs, “Overshoots in stress-strain curves:

- Colloid experiments and schematic mode coupling theory," *J. Rheol.* **57**, 149–175 (2013).
- [83] Papenkort, S., and T. Voigtmann, "Multi-scale lattice Boltzmann and mode-coupling theory calculations of the flow of a glass-forming liquid," *J. Chem. Phys.* **143**, 204502 (2015).
- [84] Nicolas, A., E. E. Ferrero, K. Martens, and J.-L. Barrat, "Deformation and flow of amorphous solids: Insights from elastoplastic models," *Rev. Mod. Phys.* **90**, 045006 (2018).
- [85] Picard, G., A. Ajdari, F. Lequeux, and L. Bocquet, "Elastic consequences of a single plastic event: A step towards the microscopic modeling of the flow of yield stress fluids," *Eur. Phys. J. E* **15**, 371–381 (2004).
- [86] Hébraud, P., and F. Lequeux, "Mode-coupling theory for the pasty rheology of soft glassy materials," *Phys. Rev. Lett.* **81**, 2934–2937 (1998).
- [87] Lin, J., and M. Wyart, "Mean-field description of plastic flow in amorphous solids," *Phys. Rev. X* **6**, 011005 (2016).
- [88] Fielding, S. M., M. E. Cates, and P. Sollich, "Shear banding, aging and noise dynamics in soft glassy materials," *Soft Matter* **5**, 2378–2382 (2009).
- [89] Hoyle, D. M., and S. M. Fielding, "Age-dependent modes of extensional necking instability in soft glassy materials," *Phys. Rev. Lett.* **114**, 158301 (2015).
- [90] Papanastasiou, T. C., "Flows of materials with yield," *J. Rheol.* **31**, 385–404 (1987).
- [91] Syrakos, A., G. C. Georgiou, and A. N. Alexandrou, "Performance of the finite volume method in solving regularised Bingham flows: Inertia effects in the lid-driven cavity flow," *J. Non-Newton. Fluid Mech.* **208**, 88–107 (2014).
- [92] Liu, B., S. Muller, and M. Denn, "Convergence of a regularization method for creeping flow of a Bingham material about a rigid sphere," *J. Non-Newton. Fluid Mech.* **102**, 179–191 (2002).
- [93] Beris, A. N., J. A. Tsamopoulos, R. C. Armstrong, and R. A. Brown, "Creeping motion of a sphere through a Bingham plastic," *J. Fluid Mech.* **158**, 219–244 (1985).
- [94] Smyrniotis, D., and J. Tsamopoulos, "Squeeze flow of Bingham plastics," *J. Non-Newton. Fluid Mech.* **100**(1–3), 165–190 (2001).
- [95] Blackery, J., and E. Mitsoulis, "Creeping motion of a sphere in tubes filled with a Bingham plastic material," *J. Non-Newton. Fluid Mech.* **70**(1–2), 59–77 (1997).
- [96] Mitsoulis, E., and J. Tsamopoulos, "Numerical simulations of complex yield-stress fluid flows," *Rheol. Acta* **56**, 231–258 (2017).
- [97] Keshavarz, B., T. Divoux, S. Manneville, and G. H. McKinley, "Nonlinear viscoelasticity and generalized failure criterion for polymer gels," *ACS Macro Lett.* **6**, 663–667 (2017).
- [98] Jaishankar, A., and G. H. McKinley, "A fractional K-BKZ constitutive formulation for describing the nonlinear rheology of multiscale complex fluids," *J. Rheol.* **58**, 1751–1788 (2014).
- [99] Wei, Y., M. J. Solomon, and R. G. Larson, "A multimode structural kinetics constitutive equation for the transient rheology of thixotropic elasto-viscoplastic fluids," *J. Rheol.* **62**, 321–342 (2018).
- [100] Wei, Y., M. J. Solomon, and R. G. Larson, "Quantitative nonlinear thixotropic model with stretched exponential response in transient shear flows," *J. Rheol.* **60**, 1301–1315 (2016).
- [101] Armstrong, M. J., A. N. Beris, S. A. Rogers, and N. J. Wagner, "Dynamic shear rheology and structure kinetics modeling of a thixotropic carbon black suspension," *Rheol. Acta* **56**, 811–824 (2017).
- [102] Saramito, P., "A new constitutive equation for elastoviscoplastic fluid flows," *J. Non-Newton. Fluid Mech.* **145**, 1–14 (2007).
- [103] de Souza Mendes, P. R., "Thixotropic elasto-viscoplastic model for structured fluids," *Soft Matter* **7**, 2471–2483 (2011).
- [104] Saramito, P., "A new elastoviscoplastic model based on the Herschel-Bulkley viscoplastic model," *J. Non-Newton. Fluid Mech.* **158**(1–3), 154–161 (2009).
- [105] Patinet, S., D. Vandembroucq, and M. L. Falk, "Connecting local yield stresses with plastic activity in amorphous solids," *Phys. Rev. Lett.* **117**, 045501 (2016).
- [106] Barbot, A., M. Lerbinger, A. Hernandez-Garcia, R. Garcia-Garcia, M. L. Falk, D. Vandembroucq, and S. Patinet, "Local yield stress statistics in model amorphous solids," *Phys. Rev. E* **97**, 033001 (2018).
- [107] Ruscher, C., and J. Rottler, [arXiv:1908.01081v3](https://arxiv.org/abs/1908.01081v3).
- [108] Sollich, P., *CECAM Workshop* (ACAM, Dublin, Ireland, 2011).
- [109] Bouchaud, J.-P., and D. S. Dean, "Aging on Parisi's tree," *J. Phys. I* **5**, 265–286 (1995).
- [110] Cates, M., and P. Sollich, "Tensorial constitutive models for disordered foams, dense emulsions, and other soft nonergodic materials," *J. Rheol.* **48**, 193–207 (2004).
- [111] Purnomo, E. H., D. van den Ende, S. A. Vanapalli, and F. Mugele, "Glass transition and aging in dense suspensions of thermosensitive microgel particles," *Phys. Rev. Lett.* **101**, 238301 (2008).
- [112] Rogers, S. A., B. M. Erwin, D. Vlassopoulos, and M. Cloitre, "A sequence of physical processes determined and quantified in LAOS: Application to a yield stress fluid," *J. Rheol.* **55**, 435–458 (2011).
- [113] Bauschinger, J., "Über die veränderung der elastizitätsgrenze und der festigkeit des eisens und stahls durch strecken und quetschen, durch erwärmen und abkühlen und durch oftmals wiederholte beanspruchung," *Mitteilungen des mechanisch-technischen Laboratoriums der Königlich Technischen Hochschule München* **13**, 1–115 (1886).
- [114] Liu, C., K. Martens, and J.-L. Barrat, "Mean-field scenario for the athermal creep dynamics of yield-stress fluids," *Phys. Rev. Lett.* **120**, 028004 (2018).